Cell Reports

Report

CRISPR screening identifies regulators of enhancer-mediated androgen receptor transcription in advanced prostate cancer

Graphical abstract

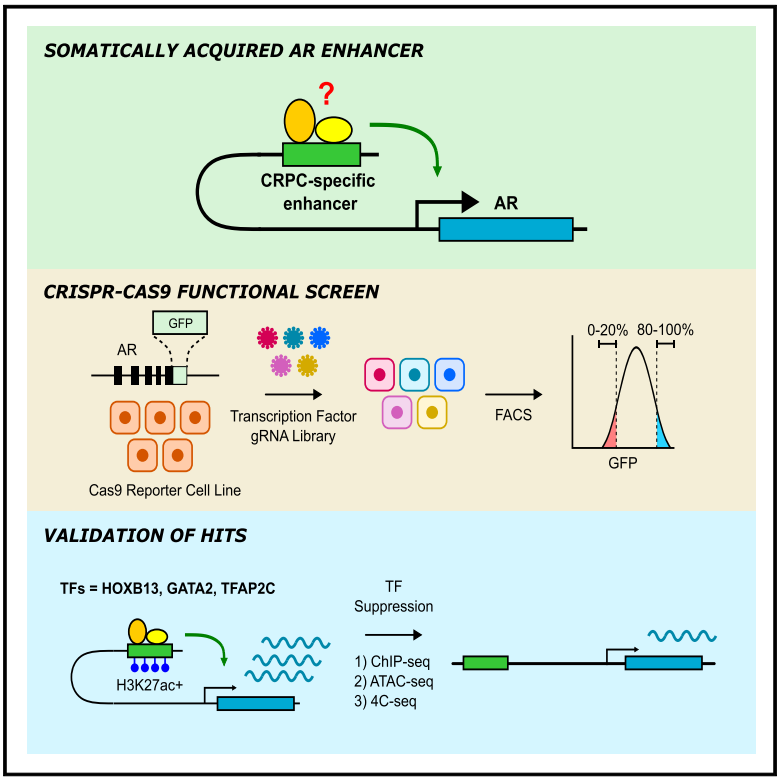

Highlights

- CRISPR screen identified HOXB13, GATA2, and TFAP2C as transcriptional regulators of AR
- HOXB13, GATA2, and TFAP2C bind the AR enhancer in multiple models of advanced prostate cancer
- Regulators promote AR enhancer H3K27 acetylation, accessibility, and enhancer-promoter looping
- AR enhancer belongs to a set of regulatory elements that require HOXB13 for FOXA1 binding

Authors

Rachel R. Xiang, Shin-Ai Lee, Caroline F. Tyndall, ..., Benjamin J. Hauk, Matthew P. Kipp, David Y. Takeda

Correspondence

david.takeda@nih.gov

In brief

The mechanism of AR enhancer activation that drives treatment resistance in advanced prostate cancers is unknown. Xiang et al. use an unbiased CRISPR screen to identify HOXB13, GATA2, and TFAP2C as regulators of enhancer-mediated AR expression and uncover insights into HOXB13-dependent reprogramming of the pioneer factor FOXA1.

Xiang et al., 2025, Cell Reports *44*, 115312
February 25, 2025 Published by Elsevier Inc.
https://doi.org/10.1016/j.celrep.2025.115312

CellPress

Cell Reports

CellPress
OPEN ACCESS

Report

CRISPR screening identifies regulators of enhancer-mediated androgen receptor transcription in advanced prostate cancer

Rachel R. Xiang,[1,2] Shin-Ai Lee,[1,2] Caroline F. Tyndall,[1] Anusha R. Bhatia,[1] JuanJuan Yin,[1] Cassandra Singler,[1] Benjamin J. Hauk,[1] Matthew P. Kipp,[1] and David Y. Takeda[1,3,*]

[1]Genitourinary Malignancies Branch, Center for Cancer Research, National Cancer Institute, National Institutes of Health, Bethesda, MD 20892, USA

[2]These authors contributed equally

[3]Lead contact

*Correspondence: david.takeda@nih.gov

https://doi.org/10.1016/j.celrep.2025.115312

SUMMARY

Amplification of the androgen receptor (AR) locus is the most frequent alteration in metastatic castration-resistant prostate cancer (CRPC). Recently, it was discovered that an enhancer of the AR is co-amplified with the AR gene body and contributes to increased AR transcription and resistance to androgen deprivation therapy. However, the mechanism of enhancer activation in advanced disease is unknown. Here, we used CRISPR-Cas9 screening to identify transcription factors that bind to the AR enhancer and modulate enhancer-mediated AR transcription. We demonstrate that HOXB13, GATA2, and TFAP2C bind the AR enhancer in patient-derived xenografts and directly impact features associated with an active chromatin state. Interestingly, the AR enhancer belongs to a set of regulatory elements that require HOXB13 to maintain FOXA1 binding, further delineating the role of HOXB13 in CRPC. This work provides a framework to functionally identify *trans*-acting factors required for the activation of disease-related noncoding regulatory elements.

INTRODUCTION

The androgen receptor (AR) remains a critical target in the treatment of prostate cancer. Therapies that suppress androgen synthesis or inhibit ligand binding to the AR are highly effective and remain the cornerstone for treating advanced disease.[1] Although the majority of patients initially respond to therapy, patients invariably relapse and develop the lethal form of prostate cancer referred to as castration-resistant prostate cancer (CRPC). A key insight into the mechanism of castration resistance was the discovery that the AR gene locus is amplified exclusively in CRPC, leading to AR overexpression that compensates for castrate androgen levels.[2,3] Subsequent experiments in laboratory models demonstrated that overexpression of AR is sufficient for castration resistance.[4] Therefore, rather than being androgen independent, CRPC is marked by the reactivation of AR signaling. This realization led to the development of potent AR signaling inhibitors (ARSis) that have significantly increased the overall survival of patients with CRPC.[5–7]

Large-scale whole-exome sequencing established that amplification of the AR locus is the most prevalent genetic alteration in CRPC, and it was assumed that the gene body was the primary target of the amplicon.[8] However, we and others identified an enhancer located 650 kb distal to AR that upregulates AR transcription and is activated exclusively in CRPC.[9–11] Closer inspection of the AR locus by whole-genome sequencing studies revealed that the AR enhancer is frequently amplified or co-amplified with the AR gene body. Intriguingly, AR enhancer copy-number gains may be more prevalent than amplification of the AR gene itself.[10–12] Duplication of the enhancer in a cell line model is sufficient to enable proliferation at low androgen concentrations and decrease sensitivity to ARSi treatment.[9] Accounting for AR enhancer amplifications, alterations affecting the AR locus occur in 80%–90% of all CRPCs,[10–12] indicating a common molecular pathway of resistance for the majority of CRPCs.

As metastatic CRPC is a ubiquitously lethal prognosis, identifying the events required for AR enhancer activation will be critical for translating our understanding of AR regulation into meaningful outcomes for patients by providing mechanistic insights to guide therapeutic strategies. Since enhancers function by recruiting *trans*-acting transcription factors, we sought to identify factors that are required for AR enhancer-mediated transcription of AR. Currently there are no robust methods to biochemically purify a specific genomic locus in order to identify associated proteins. Several approaches to combine chromatin pull-down with proteomics have been described[13–15]; however, applying these methods to low-copy-number loci is technically challenging. Furthermore, transcription factor binding does not necessarily translate to changes in transcriptional output.

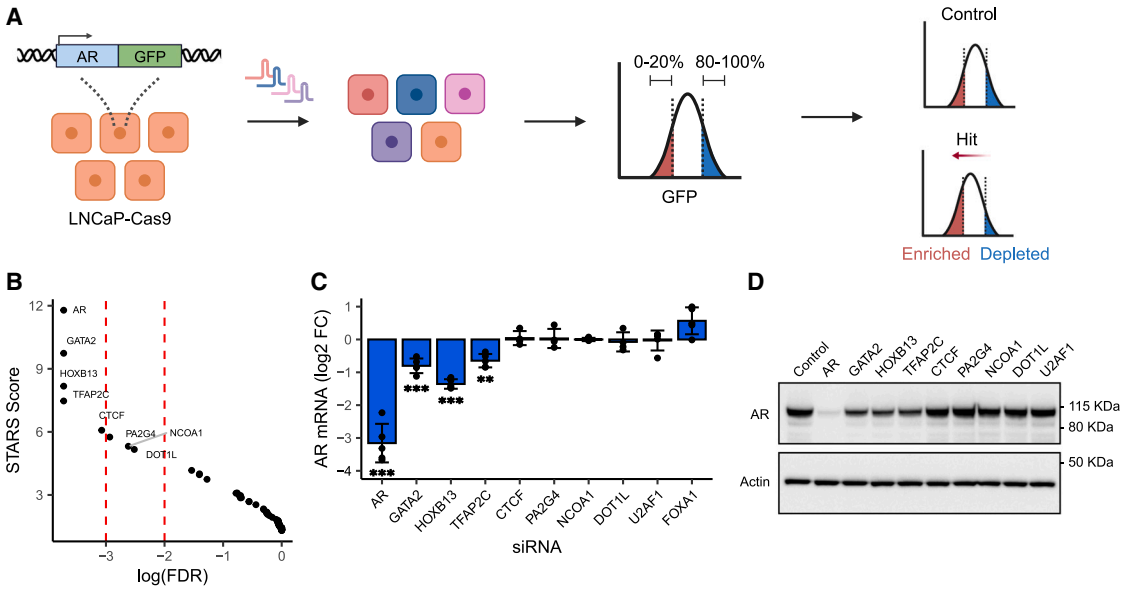

Figure 1. CRISPR-Cas9 screen identifies transcription factors that modulate AR transcription

(A) Schematic of FACS-based CRISPR-Cas9 screen targeting human transcription factors using the LNCaP cell line with GFP knocked in in the 3′ UTR of endogenous AR.

(B) Results of the screen indicating the top hits and corresponding log(false discovery rate) (log(FDR)) and STARS score. Red dashed lines indicate FDRs of 0.01 and 0.001.

(C) AR expression as determined by RT-qPCR following suppression of indicated transcription factors by siRNA. Expression is shown as log fold change relative to nontargeting control siRNA after normalization to GAPDH. Data represent the average ± standard deviation of at least 3 biological replicates, and significance was determined by a Student's t test. $^{**}p < 0.01$ and $^{***}p < 0.001$.

(D) AR protein expression as determined by immunoblotting following suppression of indicated factors by siRNA. Actin is used as a loading control.

See also Figure S1.

Therefore, we designed a functional approach to identify AR regulators in an unbiased fashion that combines CRISPR-Cas9 screening with epigenetic profiling.

RESULTS

Functional CRISPR-Cas9 screen identifies transcription factors that regulate AR expression

To identify *trans*-acting factors required for AR enhancer activity, we designed a CRISPR-Cas9 screen targeting all human transcriptions factors[16] (Figure 1A; Table S1). The LNCaP prostate cancer cell line model has an active AR enhancer that recapitulates chromatin features observed in CRPC.[9] To enable fluorescence-activated cell sorting (FACS) by AR expression, we inserted a GFP cassette at the endogenous AR locus, allowing bicistronic expression of AR and GFP. The reporter cell line was stably transduced with Cas9 and a guide RNA (gRNA) library that consisted of 4 gRNAs per factor. After allowing time for selection and gene disruption, cells were sorted by GFP intensity and individual gRNA abundance quantified by next-generation sequencing. In addition to the positive control AR, we identified transcription factors that were enriched in the low-GFP-expressing fraction (Figure 1B; Table S2). As the GFP signal was a surrogate for AR transcription, we validated hits by measuring AR mRNA directly following suppression of the candidate factors by small interfering RNA (siRNA). The top three hits, GATA2, HOXB13, and TFAP2C, suppressed AR mRNA in LNCaP cells, with HOXB13 showing the largest effect, followed by GATA2 and TFAP2C (Figures 1C and S1A). The decrease in AR mRNA was associated with a concomitant decrease in AR protein (Figure 1D). As orthogonal validation and to rule out siRNA off-target effects, we performed CRISPRi targeting the transcriptional start site of HOXB13 or TFAP2C followed by rescue with the corresponding open reading frame (Figures S1B and S1C). As we could not find suitable CRISPRi gRNAs for GATA2, we used multiple GATA2 short hairpin RNAs (shRNAs) as orthogonal validation (Figure S1D). HOXB13 is known to be involved in epigenetic reprogramming during prostate cancer tumorigenesis[17] and overexpression is associated with metastases[18]; however, direct targets of HOXB13 that contribute to disease progression are still being defined. GATA2 is amplified and overexpressed in metastatic prostate cancer, and its expression is positively correlated with AR levels.[19] GATA2 expression is also associated with worse clinical outcomes, including risk of biochemical recurrence and metastases.[19–22] However, the role of GATA2 in regulating AR expression through its distal enhancer has not been described. Although TFAP2C has not been extensively studied in prostate cancer, intriguingly, its DNA-binding motif is among those previously reported to be significantly enriched in regulatory elements that are specific to CRPC versus localized disease.[23]

To assess whether HOXB13, GATA2, and TFAP2C regulate AR in additional prostate cancer cell line models, we suppressed each factor in the AR-expressing line MDA-PCa-2b. Similar to

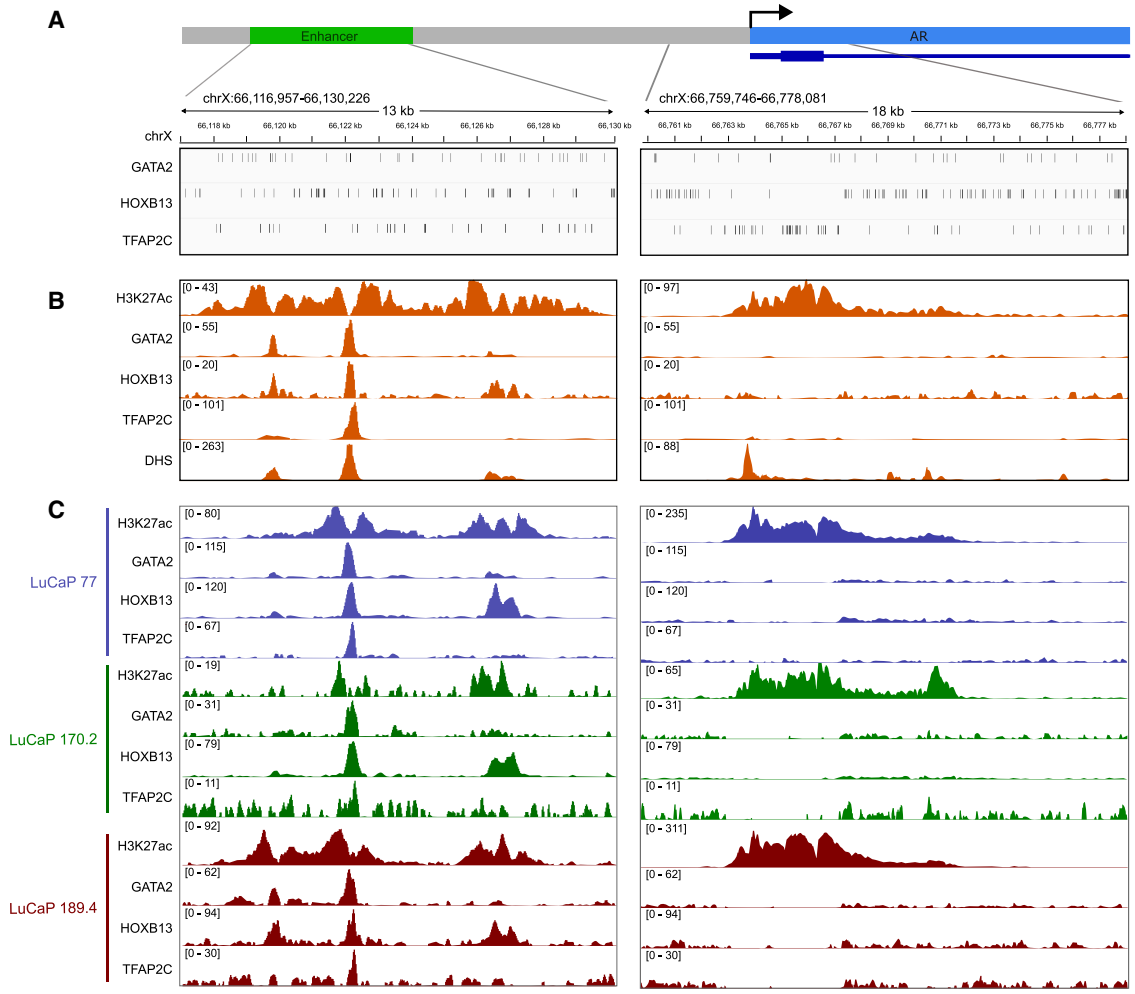

Figure 2. GATA2, HOXB13, and TFAP2C bind to the AR enhancer in cell line and patient-derived models of prostate cancer

(A) Schematic of AR enhancer and promoter (top) with locations of transcription factor binding motifs (bottom).

(B) H3K27ac and transcription factor profiles from ChIP-seq performed in LNCaP cells. The LNCaP DNaseI hypersensitivity (DHS) track was downloaded from the ENCODE project.

(C) H3K27ac and transcription factor profiles from ChIP-seq performed in indicated PDXs of metastatic prostate cancer.

See also Figure S2.

the LNCaP model, all three transcription factors significantly decreased AR expression (Figure S1E). Although FOXA1 did not score in our screen, it was included in our validation studies, as it had previously been shown to bind to the AR enhancer.[23] Consistent with our screen results, FOXA1 suppression did not decrease AR mRNA (Figures 1C and S1E), demonstrating the importance of functional validation, as transcription factor binding does not necessarily correlate with transcriptional output.

HOXB13, GATA2, and TFAP2C bind to the AR enhancer in patient-derived models of advanced prostate cancer

To determine if the candidate regulators function directly through the AR enhancer, we assessed the genome binding of GATA2, HOXB13, and TFAP2C by chromatin immunoprecipitation followed by sequencing (ChIP-seq). Motif enrichment analysis and the overlap of peaks with published datasets validated the specificity of the ChIP-seq antibodies (Figures S2A and S2B). Consistent with previous studies, ChIP-seq of the activating histone mark H3K27ac is enriched at both the enhancer and promoter of AR in LNCaP cells.[24] In contrast, ChIP-seq of GATA2, HOXB13, and TFAP2C revealed binding at the AR enhancer but not at the AR promoter, localizing their mechanism of action to the enhancer (Figures 2A and 2B). ChIP-qPCR using region-specific primers confirmed the ChIP-seq results (Figures S2C and S2D). Motif scanning revealed the presence of motifs for all transcription factors within and flanking the enhancer and promoter regions, with a subset overlapping with the ChIP-seq signal (Figure 2A). ChIP-seq profiles at the AR enhancer also correlated with chromatin accessibility based on published DNaseI hypersensitivity (DHS) data. Notably, ChIP-seq signal intensity was greatest at the second DHS peak, which was previously shown to have the most significant effect on AR transcription.[24]

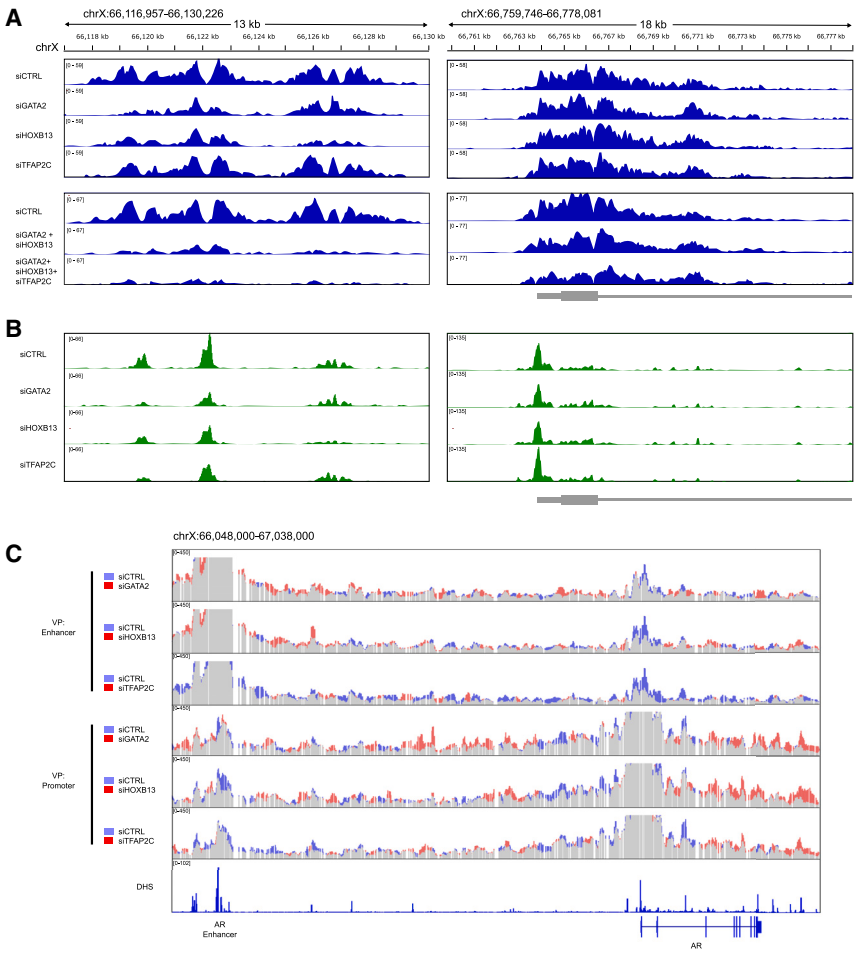

Figure 3. Candidate transcription factors affect AR enhancer acetylation, chromatin accessibility, and interaction with AR promoter

(A) ChIP-seq H3K27ac profiles in LNCaP cells at the AR enhancer (left) and promoter (right) following siRNA of indicated transcription factors or nontargeting control (siCTRL).

(B) DNA accessibility as determined by ATAC-seq in LNCaP cells at the AR enhancer (left) and promoter (right) following siRNA of indicated transcription factors or nontargeting control (siCTRL).

(C) Enhancer-promoter interactions as determined by 4C-seq anchored at the AR enhancer (VP: Enhancer) or promoter (VP: Promoter). 4C profiles represent overlays of nontargeting control siRNA (siCTRL) with indicated transcription factor siRNA. VP: 4C-seq viewpoint. The LNCaP DNaseI hypersensitivity (DHS) track was downloaded from the ENCODE project.

See also Figure S3.

To assess whether GATA2, HOXB13, and TFAP2C bind to the AR enhancer in patient-derived models of prostate cancer, we performed ChIP-seq in established patient-derived xenografts (PDXs) obtained from AR-positive metastatic CRPC.[25] In addition to the presence of H3K27ac at the AR enhancer, all three transcription factors showed binding to the AR enhancer with profiles identical to LNCaP cells (Figure 2C). The striking similarity between the pattern of transcription factor binding between LNCaP cells and PDXs further supports LNCaP cells as a model system for studying AR enhancer activity. Taken together, these results confirm that the top regulators from the screen bind to the AR enhancer in models of advanced prostate cancer.

HOXB13, GATA2, and TFAP2C impact features associated with active regulatory elements

To demonstrate that transcription factor binding has functional consequences at the AR enhancer, we examined chromatin features associated with active enhancers following the suppression of GATA2, HOXB13, and TFAP2C. Gain of the active mark H3K27ac at the AR enhancer occurs during the transition from localized to metastatic CRPC.[9,23] GATA2 and HOXB13 suppression decreased the H3K27ac signal at the enhancer compared to controls (Figure 3A). Changes in H3K27ac patterns correlated with each transcription factor's binding profile: GATA2 suppression affects H3K27ac at the first two peaks, whereas HOXB13 suppression affects H3K27ac at all three peaks. In contrast, TFAP2C suppression had a minimal effect on the H3K27ac signal. Supporting HOXB13 and GATA2 each independently contributing to H3K27ac, co-suppression of both transcription factors further decreased the H3K27ac signal. The addition of siRNA targeting TFAP2C had no further effect on H3K27ac, indicating that GATA2 and HOXB13 are primarily responsible for the enhancer H3K27ac signal. Notably, H3K27ac at the AR promoter remained unchanged, in agreement with the absence of HOXB13, GATA2, and TFAP2C binding at the promoter (Figure 3A, right).

To further localize transcription factor activity to the AR enhancer, we examined chromatin accessibility by ATAC-seq. Similar to effects on H3K27ac, the suppression of GATA2 and HOXB13 decreased accessibility at regions coincident with their binding patterns (Figure 3B). In contrast to H3K27ac, TFAP2C suppression decreased accessibility at peaks that overlap with TFAP2C binding (Figure 2B). The finding that TFAP2C affects enhancer accessibility but not H3K27ac may explain its more modest effect on modulating AR expression.

Since distal enhancers physically interact with their target genes in three-dimensional space to activate transcription, we investigated whether the candidate factors influence enhancer-promoter interactions using 4C-seq. Despite being 650 kb upstream of the AR promoter, there is increased interaction frequency between the AR enhancer and the 5′ end of the AR gene (Figure 3C), consistent with previous results using 3C,[9] Hi-C,[26,27] and ChIA-PET.[28] Suppression of GATA2, HOXB13, or TFAP2C decreased enhancer-promoter interactions, indicating a role in mediating enhancer-promoter looping (Figure 3C).

Intriguingly, the decrease in enhancer-promoter contacts is associated with an increase in interactions outside the enhancer and promoter regions. In summary, the ChIP-seq, ATAC-seq, and 4C-seq results demonstrate that GATA2, HOXB13, and TFAP2C alter epigenetic features associated with active regulatory elements, supporting their functional role in regulating AR transcription through its distal enhancer.

HOXB13, GATA2, and TFAP2C regulate AR in CRPC models treated with ARSi

To investigate the role of the candidate transcription factors in ARSi-treated CRPC, we suppressed HOXB13, GATA2, and TFAP2C in the enzalutamide-resistant VCaP16 cell line.[29] VCaP16 cells express the AR-V7 splice variant, which is frequently upregulated in patients treated with ARSis.[30–33] AR-V7 retains transcription activation activity but lacks the ligand-binding domain (LBD) that interacts with enzalutamide. The suppression of HOXB13, GATA2, or TFAP2C decreased the expression of both full-length AR and AR-V7 (Figures S3A and S3B), confirming that targeting the AR enhancer is a potential strategy for decreasing the transcription of splice variants that contribute to resistance. All three transcription factors bind to the AR enhancer with a profile comparable to LNCaP cells and PDXs (Figure S3C). Similar to LNCaP cells, the suppression of HOXB13 and GATA2 decreased H3K27ac at the AR enhancer. We identified H3K27ac peaks outside the AR enhancer that are located more proximal to the AR gene (Figure S3C, proximal 1–4). These sites showed variable HOXB13 and GATA2 binding and decreased H3K27ac signal following suppression of the corresponding overlapping factor. However, the distal AR enhancer demonstrates the greatest signal density and is the only region that binds all three transcription factors. Although we cannot rule out the presence of additional enhancers that contribute to AR transcription, the prominent role of the distal enhancer is supported by genomic data showing recurrent focal amplifications of the distal AR enhancer[10,11,34] and functional data demonstrating that the suppression of the distal AR enhancer decreases viability, while amplification is sufficient to confer a castration-resistant phenotype.[9]

AR enhancer belongs to a class of enhancers characterized by HOXB13 programming of FOXA1

We next investigated whether our focused interrogation of the AR enhancer could provide insight into the genome-wide enhancer reprogramming that occurs during the transition to CRPC. Although both HOXB13 and GATA2 modulated H3K27ac at the AR enhancer, we were surprised to find that the suppression of HOXB13 had a more dramatic effect on the H3K27ac landscape, with changes in 9,068 peaks versus 814 peaks with GATA2 (Figure 4A). As observed with the AR enhancer, TFAP2C suppression did not significantly alter H3K27ac genome wide. Pairwise correlation of H3K27ac profiles confirmed that GATA2 and TFAP2C suppression clustered more closely with the control siRNA than with HOXB13 suppression (Figure 4B). The H3K27ac profile following HOXB13 suppression also clustered with concurrent suppression of all three factors, indicating that the changes in H3K27ac are driven primarily by HOXB13. In stark contrast, changes in gene expression as determined by RNA sequencing (RNA-seq) showed 864 differentially regulated genes following GATA2 suppression, comparable to 1,114 genes with HOXB13 (Figure S4A). Unsupervised clustering also showed that GATA2 formed a distinct cluster from HOXB13, TFAP2C, and control siRNAs (Figure 4C). Despite TFAP2C having the fewest differentially regulated genes, gene set enrichment analysis (GSEA) indicated that the most significantly downregulated gene set is ANDROGEN_RESPONSE (Figure S4A), supporting its role in regulating AR transcription. These results indicate that HOXB13 alters both the transcriptome and enhancer landscape, while GATA2 and TFAP2C modulate transcriptional programs without extensive changes in H3K27ac.

To relate HOXB13-dependent effects on the enhancer landscape with gene expression, we used a previously published HiChIP dataset[35] to map H3K27ac peaks to target genes. GSEA confirmed that genes mapped to significantly decreased H3K27ac peaks following HOXB13 suppression also had decreased RNA expression (Figure S4B). Gene Ontology enrichment analysis of the mapped genes identified terms associated with hormone signaling as well as terms associated with development, such as pattern specification, embryonic organ development, and anterior-posterior pattern specification (Figure S4C). These findings provide functional validation for previous observations that CRPC is associated with activation of fetal developmental programs involving HOXB13 enhancer reprogramming[23] and support the hypothesis that the AR enhancer is a dormant developmental enhancer that is reactivated in CRPC.[9]

To further investigate changes in the enhancer landscape following HOXB13 suppression, we performed a motif enrichment of regions with significant changes in H3K27ac (Figure 4D). Sites with decreased H3K27ac were enriched for HOXB13 and FOXA1 binding motifs as expected; however, sites with increased H3K27ac were strongly enriched for the FOXA1 motif only (Figure 4E). To determine if HOXB13 loss reprograms the FOXA1 cistrome, we performed FOXA1 ChIP-seq following HOXB13 suppression and discovered the global redistribution of FOXA1, with reduced occupancy at H3K27ac lost sites and increased binding at H3K27ac gained sites (Figure 4F). Inspection of the AR enhancer confirmed decreased FOXA1 occupancy following the suppression of HOXB13 (Figure S4D). H3K27ac lost sites were also associated with decreased chromatin accessibility and gained sites with increased accessibility by ATAC-seq (Figure S4E), further supporting reprogramming of the enhancer landscape. We confirmed that the HOXB13-dependent changes in H3K27ac were not due to indirect effects of decreased AR expression by comparing the suppression of HOXB13 to AR (Figure S4F). Therefore, the AR enhancer belongs to a set of regulatory elements that depend on HOXB13 for H3K27ac, chromatin accessibility, and FOXA1 binding.

DISCUSSION

The near-universal amplification of AR in CRPC underscores its importance in mediating castration resistance. Current methods to target AR reactivation include decreasing circulating levels of androgens or competing with androgen binding to the LBD of AR. However, there are no FDA-approved therapies that target AR transcription itself. The AR enhancer provides a potential opportunity to directly target AR transcription in CRPC. Additional

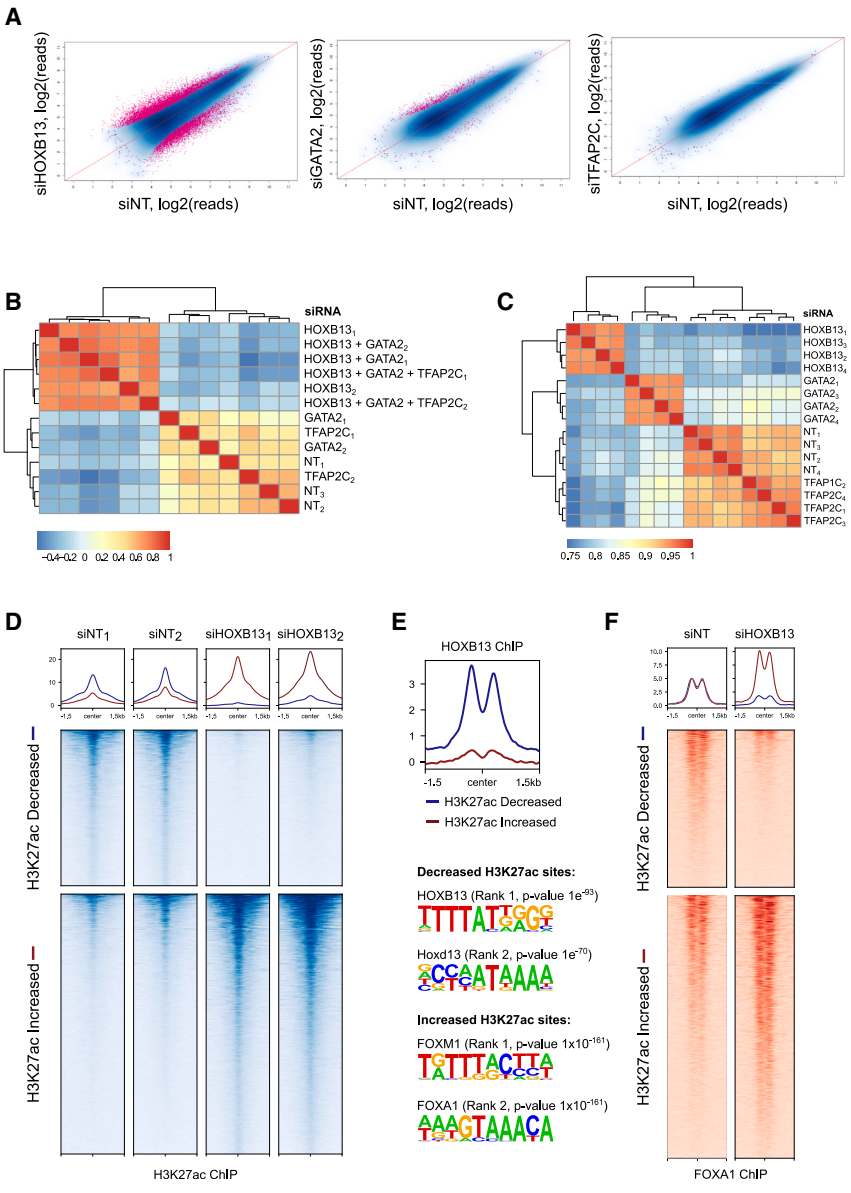

Figure 4. HOXB13 loss causes genome-wide enhancer and FOXA1 reprogramming

(A) Scatterplot of H3K27ac ChIP-seq peaks after treatment with indicated siRNAs. Differential peaks with FDRs <0.05 are indicated in magenta.

(B) Correlation heatmap of H3K27ac peaks following suppression of indicated transcription factors by siRNA or a nontargeting (NT) control. Subscript indicates the replicate number.

(C) Correlation heatmap of gene expression as determined by RNA-seq following suppression by the indicated siRNA.

(D) Profile plots and heatmaps of H3K27ac signal at regions that were significantly decreased or increased by HOXB13 suppression.

(E) Profile plot of average HOXB13 ChIP-seq signal (top) and top enriched motifs (bottom) at H3K27ac sites that show significant decreased or increased signals.

(F) Profile plot and heatmap of FOXA1 ChIP-seq signal at H3K27ac decreased and increased sites. See also Figure S4.

mechanisms of resistance to current ARSis, such as AR LBD mutations or splice variants that delete the LBD, would also be susceptible to therapies that inhibit AR transcription.[30,31,36] Therefore, identifying factors required for AR enhancer activity provides targets for novel therapies that overcome multiple resistance mechanisms. Toward this goal, we used an unbiased functional screening approach coupled with epigenomic profiling to discover that HOXB13, GATA2, and TFAP2C bind to the AR enhancer and modulate AR transcription in multiple prostate cancer models, including an ARSi-resistant model, which expresses the AR splice variant AR-V7. We were particularly interested in identifying factors that impact chromatin modifications, as CRPC is distinguished by a gain in H3K27ac at the AR enhancer. Although all three regulators affect chromatin accessibility at the enhancer and enhancer-promoter interactions, only HOXB13 and GATA2 affect H3K27ac.

HOXB13 and GATA2 have been previously shown to play a role in prostate cancer tumorigenesis and disease progression; however, these results are the first to demonstrate their role in directly mediating AR expression through its somatically acquired enhancer.

Genetic variants of HOXB13 are associated with a significant increase in the risk of prostate cancer,[37] however, the mechanism remains unclear. Recently it was shown that the HOXB13 G84E risk variant influences lipogenesis through recruitment of HDAC3.[38] HOXB13 has also been previously implicated in regulating response to androgens[39,40] and activity of AR splice variants.[41] Here we show that HOXB13 contributes to castration-resistance through regulation of AR transcription. Although the AR enhancer is inactive in localized disease based on the absence of H3K27ac, there is evidence of HOXB13 occupancy suggesting that HOXB13 binding is insufficient for AR enhancer activation. Our results are consistent with these observations as GATA2 and TFAP2C are necessary for maximal H3K27ac and AR expression. We hypothesize that HOXB13 epigenetically bookmarks the AR enhancer for subsequent activation by transcription factors that are upregulated during the transition to castration-resistance. By modulating AR enhancer-promoter interactions, HOXB13 could also play a role in maintaining chromatin architecture in a poised state. These findings raise the intriguing possibility of pre-emptively preventing enhancer activation by targeting HOXB13 before or concurrently with androgen-directed therapies. Although transcription factors have been historically difficult to target with small molecules, the development of molecular glues and

PROTAC technology now makes it feasible to target specific transcription factors.

Although we focused on the AR enhancer given its prominent role in castration resistance, its activation is part of a global reprogramming process associated with CRPC. Therefore, understanding determinants of AR enhancer activity may provide insight into the mechanism of epigenetic reprogramming genome wide. We discovered that the suppression of HOXB13 results in widespread changes in the pattern of H3K27ac and chromatin accessibility. Analogous to AR, the expression of genes that physically interact with these regulatory elements is downregulated by HOXB13 suppression. In addition to androgen signaling, these genes are enriched for embryonic developmental programs, supporting the previous observation that the CRPC epigenome resembles fetal prostate tissue.[23] Motif analysis of gained and lost H3K27ac sites indicated reprogramming of FOXA1, which is frequently mutated in prostate cancer and contributes to tumorigenesis.[17,42,43] Although FOXA1 belongs to the class of transcription factors referred to as pioneer factors that have the ability to access closed chromatin, the suppression of HOXB13 causes redistribution from HOXB13 and FOXA1 co-occupied sites to FOXA1-only sites. This previously unknown function of HOXB13 to regulate FOXA1 binding further demonstrates the critical role of HOXB13 in reprogramming the CRPC epigenetic landscape and its potential as a therapeutic target.

Limitations of the study

Although we identified transcription factors required for enhancer-mediated AR transcription, a limitation of our study is being able to show the activation of an inactive enhancer due to the lack of available models of localized prostate cancers. There are no localized prostate cancer cell line models, and nearly all PDXs and organoids amenable to *in vitro* studies are from metastatic lesions, highlighting the historical difficulties in generating diverse prostate cancer models. Newer techniques to profile different epigenetic marks from cell-free plasma[44–47] may provide opportunities in the future to examine serial samples from patients during the transition from castration-sensitive to -resistant disease.

RESOURCE AVAILABILITY

Lead contact

Requests for further information and resources should be directed to and will be fulfilled by the lead contact, David Y. Takeda (david.takeda@nih.gov).

Materials availability

All reagents generated in this study are available from the lead contact with a completed materials transfer agreement.

Data and code availability

- Raw ChIP-seq, RNA-seq, ATAC-seq, and 4C-seq data have been deposited in GEO under accession GEO: GSE276052 and are publicly available.
- Custom code is deposited at Zenodo: https://doi.org/10.5281/zenodo.14721032 and is publicly available.
- Any additional information required to reanalyze the data reported in this paper is available from the lead contact upon request.

ACKNOWLEDGMENTS

This work was supported by the Intramural Research Program of the NIH, United States (ZIABC011965). The authors would like to thank Kathleen Kelly, Adam Sowalsky, and members of the Takeda Laboratory for useful discussions and technical assistance. Next-generation sequencing was done at the CCR Genomics Core at the National Cancer Institute, NIH, Bethesda, MD. This work utilized the computational resources of the NIH HPC Biowulf cluster (https://hpc.nih.gov).

AUTHOR CONTRIBUTIONS

Conceptualization, R.R.X., S.-A.L., and D.Y.T.; methodology, R.R.X., S.-A.L., C.F.T., A.R.B., J.Y., C.S., B.J.H., M.P.K., and D.Y.T.; formal analysis, R.R.X., S.-A.L., C.F.T., A.R.B., C.S., B.J.H., M.P.K., and D.Y.T.; investigation, R.R.X., S.-A.L., C.F.T., A.R.B., J.Y., C.S., M.P.K., and D.Y.T.; writing – original draft, R.R.X., S.-A.L., C.F.T., and D.Y.T.; writing – review & editing, R.R.X., S.-A.L., and D.Y.T.; resources, D.Y.T.; supervision, D.Y.T.

DECLARATION OF INTERESTS

The authors declare no competing interests.

STAR★METHODS

Detailed methods are provided in the online version of this paper and include the following:

- KEY RESOURCES TABLE
- EXPERIMENTAL MODEL AND STUDY PARTICIPANT DETAILS
  - Cell lines
  - PDX samples
- METHOD DETAILS
  - Creation of reporter cell line LNCaP-AR-GFP
  - Design and creation of transcription factor gRNA library
  - Pooled lentivirus CRISPR screen for *trans*-acting factors
  - Analysis of Pooled Screen Data
  - siRNA experiments
  - CRISRPi rescue experiments
  - shRNA experiments
  - Quantitative RT-PCR
  - Immunoblotting
  - Cell line and tissue ChIP
  - ATAC-seq
  - RNA-seq
  - ChIP-seq and ATAC-seq data analysis
  - Scanning motif analysis
  - 4C-seq
  - Linking HiChIP data to genes
- QUANTIFICATION AND STATISTICAL ANALYSES
  - CRISPR-Cas9 screen
  - Quantitative RT-PCR experiments
  - ChIP-seq and ATAC-seq experiments
  - RNA-seq experiments

SUPPLEMENTAL INFORMATION

Supplemental information can be found online at https://doi.org/10.1016/j.celrep.2025.115312.

Received: September 12, 2024
Revised: December 17, 2024
Accepted: January 23, 2025
Published: February 14, 2025

REFERENCES

1. Crawford, E.D., Heidenreich, A., Lawrentschuk, N., Tombal, B., Pompeo, A.C.L., Mendoza-Valdes, A., Miller, K., Debruyne, F.M.J., and Klotz, L. (2019). Androgen-targeted therapy in men with prostate cancer: evolving practice and future considerations. Prostate Cancer Prostatic Dis. *22*, 24–38. https://doi.org/10.1038/s41391-018-0079-0.
2. Visakorpi, T., Hyytinen, E., Koivisto, P., Tanner, M., Keinänen, R., Palmberg, C., Palotie, A., Tammela, T., Isola, J., and Kallioniemi, O.P. (1995). In vivo amplification of the androgen receptor gene and progression of human prostate cancer. Nat. Genet. *9*, 401–406. https://doi.org/10.1038/ng0495-401.
3. Robinson, D., Van Allen, E.M., Wu, Y.M., Schultz, N., Lonigro, R.J., Mosquera, J.M., Montgomery, B., Taplin, M.E., Pritchard, C.C., Attard, G., et al. (2015). Integrative clinical genomics of advanced prostate cancer. Cell *161*, 1215–1228. https://doi.org/10.1016/j.cell.2015.05.001.
4. Chen, C.D., Welsbie, D.S., Tran, C., Baek, S.H., Chen, R., Vessella, R., Rosenfeld, M.G., and Sawyers, C.L. (2004). Molecular determinants of resistance to antiandrogen therapy. Nat. Med. *10*, 33–39. https://doi.org/10.1038/nm972.
5. Tran, C., Ouk, S., Clegg, N.J., Chen, Y., Watson, P.A., Arora, V., Wongvipat, J., Smith-Jones, P.M., Yoo, D., Kwon, A., et al. (2009). Development of a second-generation antiandrogen for treatment of advanced prostate cancer. Science *324*, 787–790. https://doi.org/10.1126/science.1168175.
6. Scher, H.I., Fizazi, K., Saad, F., Taplin, M.E., Sternberg, C.N., Miller, K., de Wit, R., Mulders, P., Chi, K.N., Shore, N.D., et al. (2012). Increased survival with enzalutamide in prostate cancer after chemotherapy. N. Engl. J. Med. *367*, 1187–1197. https://doi.org/10.1056/NEJMoa1207506.
7. de Bono, J.S., Logothetis, C.J., Molina, A., Fizazi, K., North, S., Chu, L., Chi, K.N., Jones, R.J., Goodman, O.B., Jr., Saad, F., et al. (2011). Abiraterone and increased survival in metastatic prostate cancer. N. Engl. J. Med. *364*, 1995–2005. https://doi.org/10.1056/NEJMoa1014618.
8. Armenia, J., Wankowicz, S.A.M., Liu, D., Gao, J., Kundra, R., Reznik, E., Chatila, W.K., Chakravarty, D., Han, G.C., Coleman, I., et al. (2018). The long tail of oncogenic drivers in prostate cancer. Nat. Genet. *50*, 645–651. https://doi.org/10.1038/s41588-018-0078-z.
9. Takeda, D.Y., Spisak, S., Seo, J.H., Bell, C., O'Connor, E., Korthauer, K., Ribli, D., Csabai, I., Solymosi, N., Szallasi, Z., et al. (2018). A Somatically Acquired Enhancer of the Androgen Receptor Is a Noncoding Driver in Advanced Prostate Cancer. Cell *174*, 422–432. https://doi.org/10.1016/j.cell.2018.05.037.
10. Viswanathan, S.R., Ha, G., Hoff, A.M., Wala, J.A., Carrot-Zhang, J., Whelan, C.W., Haradhvala, N.J., Freeman, S.S., Reed, S.C., Rhoades, J., et al. (2018). Structural Alterations Driving Castration-Resistant Prostate Cancer Revealed by Linked-Read Genome Sequencing. Cell *174*, 433–447. https://doi.org/10.1016/j.cell.2018.05.036.
11. Quigley, D.A., Dang, H.X., Zhao, S.G., Lloyd, P., Aggarwal, R., Alumkal, J.J., Foye, A., Kothari, V., Perry, M.D., Bailey, A.M., et al. (2018). Genomic Hallmarks and Structural Variation in Metastatic Prostate Cancer. Cell *174*, 758–769.e9. https://doi.org/10.1016/j.cell.2018.06.039.
12. Zhou, M., Ko, M., Hoge, A.C., Luu, K., Liu, Y., Russell, M.L., Hannon, W.W., Zhang, Z., Carrot-Zhang, J., Beroukhim, R., et al. (2022). Patterns of structural variation define prostate cancer across disease states. JCI Insight *7*, e161370. https://doi.org/10.1172/jci.insight.161370.
13. Déjardin, J., and Kingston, R.E. (2009). Purification of proteins associated with specific genomic Loci. Cell *136*, 175–186. https://doi.org/10.1016/j.cell.2008.11.045.
14. Myers, S.A., Wright, J., Peckner, R., Kalish, B.T., Zhang, F., and Carr, S.A. (2018). Discovery of proteins associated with a predefined genomic locus via dCas9-APEX-mediated proximity labeling. Nat. Methods *15*, 437–439. https://doi.org/10.1038/s41592-018-0007-1.
15. Gao, X.D., Tu, L.C., Mir, A., Rodriguez, T., Ding, Y., Leszyk, J., Dekker, J., Shaffer, S.A., Zhu, L.J., Wolfe, S.A., and Sontheimer, E.J. (2018). C-BERST: defining subnuclear proteomic landscapes at genomic elements with dCas9-APEX2. Nat. Methods *15*, 433–436. https://doi.org/10.1038/s41592-018-0006-2.
16. Lambert, S.A., Jolma, A., Campitelli, L.F., Das, P.K., Yin, Y., Albu, M., Chen, X., Taipale, J., Hughes, T.R., and Weirauch, M.T. (2018). The Human Transcription Factors. Cell *172*, 650–665. https://doi.org/10.1016/j.cell.2018.01.029.
17. Pomerantz, M.M., Li, F., Takeda, D.Y., Lenci, R., Chonkar, A., Chabot, M., Cejas, P., Vazquez, F., Cook, J., Shivdasani, R.A., et al. (2015). The androgen receptor cistrome is extensively reprogrammed in human prostate tumorigenesis. Nat. Genet. *47*, 1346–1351. https://doi.org/10.1038/ng.3419.
18. Zabalza, C.V., Adam, M., Burdelski, C., Wilczak, W., Wittmer, C., Kraft, S., Krech, T., Steurer, S., Koop, C., Hube-Magg, C., et al. (2015). HOXB13 overexpression is an independent predictor of early PSA recurrence in prostate cancer treated by radical prostatectomy. Oncotarget *6*, 12822–12834. https://doi.org/10.18632/oncotarget.3431.
19. He, B., Lanz, R.B., Fiskus, W., Geng, C., Yi, P., Hartig, S.M., Rajapakshe, K., Shou, J., Wei, L., Shah, S.S., et al. (2014). GATA2 facilitates steroid receptor coactivator recruitment to the androgen receptor complex. Proc. Natl. Acad. Sci. USA *111*, 18261–18266. https://doi.org/10.1073/pnas.1421415111.
20. Yang, X., Zhang, Q., Li, S., Devarajan, R., Luo, B., Tan, Z., Wang, Z., Giannareas, N., Wenta, T., Ma, W., et al. (2023). GATA2 co-opts TGFβ1/SMAD4 oncogenic signaling and inherited variants at 6q22 to modulate prostate cancer progression. J. Exp. Clin. Cancer Res. *42*, 198. https://doi.org/10.1186/s13046-023-02745-7.
21. Böhm, M., Locke, W.J., Sutherland, R.L., Kench, J.G., and Henshall, S.M. (2009). A role for GATA-2 in transition to an aggressive phenotype in prostate cancer through modulation of key androgen-regulated genes. Oncogene *28*, 3847–3856. https://doi.org/10.1038/onc.2009.243.
22. Chiang, Y.T., Wang, K., Fazli, L., Qi, R.Z., Gleave, M.E., Collins, C.C., Gout, P.W., and Wang, Y. (2014). GATA2 as a potential metastasis-driving gene in prostate cancer. Oncotarget *5*, 451–461. https://doi.org/10.18632/oncotarget.1296.
23. Pomerantz, M.M., Qiu, X., Zhu, Y., Takeda, D.Y., Pan, W., Baca, S.C., Gusev, A., Korthauer, K.D., Severson, T.M., Ha, G., et al. (2020). Prostate cancer reactivates developmental epigenomic programs during metastatic progression. Nat. Genet. *52*, 790–799. https://doi.org/10.1038/s41588-020-0664-8.
24. Baca, S.C., Takeda, D.Y., Seo, J.H., Hwang, J., Ku, S.Y., Arafeh, R., Arnoff, T., Agarwal, S., Bell, C., O'Connor, E., et al. (2021). Reprogramming of the FOXA1 cistrome in treatment-emergent neuroendocrine prostate cancer. Nat. Commun. *12*, 1979. https://doi.org/10.1038/s41467-021-22139-7.
25. Nguyen, H.M., Vessella, R.L., Morrissey, C., Brown, L.G., Coleman, I.M., Higano, C.S., Mostaghel, E.A., Zhang, X., True, L.D., Lam, H.M., et al. (2017). LuCaP Prostate Cancer Patient-Derived Xenografts Reflect the Molecular Heterogeneity of Advanced Disease an–d Serve as Models for Evaluating Cancer Therapeutics. Prostate *77*, 654–671. https://doi.org/10.1002/pros.23313.
26. Rhie, S.K., Perez, A.A., Lay, F.D., Schreiner, S., Shi, J., Polin, J., and Farnham, P.J. (2019). A high-resolution 3D epigenomic map reveals insights into the creation of the prostate cancer transcriptome. Nat. Commun. *10*, 4154. https://doi.org/10.1038/s41467-019-12079-8.
27. San Martin, R., Das, P., Dos Reis Marques, R., Xu, Y., Roberts, J.M., Sanders, J.T., Golloshi, R., and McCord, R.P. (2022). Chromosome compartmentalization alterations in prostate cancer cell lines model disease progression. J. Cell Biol. *221*, e202104108. https://doi.org/10.1083/jcb.202104108.
28. Ramanand, S.G., Chen, Y., Yuan, J., Daescu, K., Lambros, M.B., Houlahan, K.E., Carreira, S., Yuan, W., Baek, G., Sharp, A., et al. (2020). The landscape of RNA polymerase II-associated chromatin interactions in prostate cancer. J. Clin. Invest. *130*, 3987–4005. https://doi.org/10.1172/JCI134260.

29. Poluben, L., Nouri, M., Liang, J., Chen, S., Varkaris, A., Ersoy-Fazlioglu, B., Voznesensky, O., Lee, I.I., Qiu, X., Cato, L., et al. (2024). Increased nuclear factor I-mediated chromatin access drives transition to androgen receptor splice variant dependence in prostate cancer. Cell Rep. *44*, 115089. https://doi.org/10.1016/j.celrep.2024.115089.

30. Antonarakis, E.S., Lu, C., Wang, H., Luber, B., Nakazawa, M., Roeser, J.C., Chen, Y., Mohammad, T.A., Chen, Y., Fedor, H.L., et al. (2014). AR-V7 and resistance to enzalutamide and abiraterone in prostate cancer. N. Engl. J. Med. *371*, 1028–1038. https://doi.org/10.1056/NEJMoa1315815.

31. Dehm, S.M., Schmidt, L.J., Heemers, H.V., Vessella, R.L., and Tindall, D.J. (2008). Splicing of a novel androgen receptor exon generates a constitutively active androgen receptor that mediates prostate cancer therapy resistance. Cancer Res. *68*, 5469–5477. https://doi.org/10.1158/0008-5472.CAN-08-0594.

32. Armstrong, A.J., Halabi, S., Luo, J., Nanus, D.M., Giannakakou, P., Szmulewitz, R.Z., Danila, D.C., Healy, P., Anand, M., Rothwell, C.J., et al. (2019). Prospective Multicenter Validation of Androgen Receptor Splice Variant 7 and Hormone Therapy Resistance in High-Risk Castration-Resistant Prostate Cancer: The PROPHECY Study. J. Clin. Oncol. *37*, 1120–1129. https://doi.org/10.1200/JCO.18.01731.

33. Sharp, A., Coleman, I., Yuan, W., Sprenger, C., Dolling, D., Rodrigues, D.N., Russo, J.W., Figueiredo, I., Bertan, C., Seed, G., et al. (2019). Androgen receptor splice variant-7 expression emerges with castration resistance in prostate cancer. J. Clin. Invest. *129*, 192–208. https://doi.org/10.1172/JCI122819.

34. Herberts, C., Annala, M., Sipola, J., Ng, S.W.S., Chen, X.E., Nurminen, A., Korhonen, O.V., Munzur, A.D., Beja, K., Schönlau, E., et al. (2022). Deep whole-genome ctDNA chronology of treatment-resistant prostate cancer. Nature *608*, 199–208. https://doi.org/10.1038/s41586-022-04975-9.

35. Giambartolomei, C., Seo, J.H., Schwarz, T., Freund, M.K., Johnson, R.D., Spisak, S., Baca, S.C., Gusev, A., Mancuso, N., Pasaniuc, B., and Freedman, M.L. (2021). H3K27ac HiChIP in prostate cell lines identifies risk genes for prostate cancer susceptibility. Am. J. Hum. Genet. *108*, 2284–2300. https://doi.org/10.1016/j.ajhg.2021.11.007.

36. Taplin, M.E., Bubley, G.J., Shuster, T.D., Frantz, M.E., Spooner, A.E., Ogata, G.K., Keer, H.N., and Balk, S.P. (1995). Mutation of the androgen-receptor gene in metastatic androgen-independent prostate cancer. N. Engl. J. Med. *332*, 1393–1398. https://doi.org/10.1056/NEJM199505253322101.

37. Ewing, C.M., Ray, A.M., Lange, E.M., Zuhlke, K.A., Robbins, C.M., Tembe, W.D., Wiley, K.E., Isaacs, S.D., Johng, D., Wang, Y., et al. (2012). Germline mutations in HOXB13 and prostate-cancer risk. N. Engl. J. Med. *366*, 141–149. https://doi.org/10.1056/NEJMoa1110000.

38. Lu, X., Fong, K.W., Gritsina, G., Wang, F., Baca, S.C., Brea, L.T., Berchuck, J.E., Spisak, S., Ross, J., Morrissey, C., et al. (2022). HOXB13 suppresses de novo lipogenesis through HDAC3-mediated epigenetic reprogramming in prostate cancer. Nat. Genet. *54*, 670–683. https://doi.org/10.1038/s41588-022-01045-8.

39. Norris, J.D., Chang, C.Y., Wittmann, B.M., Kunder, R.S., Cui, H., Fan, D., Joseph, J.D., and McDonnell, D.P. (2009). The homeodomain protein HOXB13 regulates the cellular response to androgens. Mol. Cell *36*, 405–416. https://doi.org/10.1016/j.molcel.2009.10.020.

40. Kim, E.H., Cao, D., Mahajan, N.P., Andriole, G.L., and Mahajan, K. (2020). ACK1-AR and AR-HOXB13 signaling axes: epigenetic regulation of lethal prostate cancers. NAR Cancer *2*, zcaa018. https://doi.org/10.1093/narcan/zcaa018.

41. Chen, Z., Wu, D., Thomas-Ahner, J.M., Lu, C., Zhao, P., Zhang, Q., Geraghty, C., Yan, P.S., Hankey, W., Sunkel, B., et al. (2018). Diverse AR-V7 cistromes in castration-resistant prostate cancer are governed by HoxB13. Proc. Natl. Acad. Sci. USA *115*, 6810–6815. https://doi.org/10.1073/pnas.1718811115.

42. Parolia, A., Cieslik, M., Chu, S.C., Xiao, L., Ouchi, T., Zhang, Y., Wang, X., Vats, P., Cao, X., Pitchiaya, S., et al. (2019). Distinct structural classes of activating FOXA1 alterations in advanced prostate cancer. Nature *571*, 413–418. https://doi.org/10.1038/s41586-019-1347-4.

43. Adams, E.J., Karthaus, W.R., Hoover, E., Liu, D., Gruet, A., Zhang, Z., Cho, H., DiLoreto, R., Chhangawala, S., Liu, Y., et al. (2019). FOXA1 mutations alter pioneering activity, differentiation and prostate cancer phenotypes. Nature *571*, 408–412. https://doi.org/10.1038/s41586-019-1318-9.

44. Sadeh, R., Sharkia, I., Fialkoff, G., Rahat, A., Gutin, J., Chappleboim, A., Nitzan, M., Fox-Fisher, I., Neiman, D., Meler, G., et al. (2021). ChIP-seq of plasma cell-free nucleosomes identifies gene expression programs of the cells of origin. Nat. Biotechnol. *39*, 586–598. https://doi.org/10.1038/s41587-020-00775-6.

45. Pongor, L.S., Schultz, C.W., Rinaldi, L., Wangsa, D., Redon, C.E., Takahashi, N., Fialkoff, G., Desai, P., Zhang, Y., Burkett, S., et al. (2023). Extrachromosomal DNA Amplification Contributes to Small Cell Lung Cancer Heterogeneity and Is Associated with Worse Outcomes. Cancer Discov. *13*, 928–949. https://doi.org/10.1158/2159-8290.CD-22-0796.

46. El Zarif, T., Semaan, K., Eid, M., Seo, J.H., Garinet, S., Davidsohn, M.P., Sahgal, P., Fortunato, B., Canniff, J., Nassar, A.H., et al. (2024). Epigenomic signatures of sarcomatoid differentiation to guide the treatment of renal cell carcinoma. Cell Rep. *43*, 114350. https://doi.org/10.1016/j.celrep.2024.114350.

47. Sipola, J., Munzur, A.D., Kwan, E.M., Seo, C.C.Y., Hauk, B.J., Parekh, K., Liao, Y.J.R., Bernales, C.Q., Donnellan, G., Bloise, I., et al. (2024). Plasma cell-free DNA chromatin immunoprecipitation profiling depicts phenotypic and clinical heterogeneity in advanced prostate cancer. Cancer Res. https://doi.org/10.1158/0008-5472.CAN-24-2052.

48. Cong, L., Ran, F.A., Cox, D., Lin, S., Barretto, R., Habib, N., Hsu, P.D., Wu, X., Jiang, W., Marraffini, L.A., and Zhang, F. (2013). Multiplex genome engineering using CRISPR/Cas systems. Science *339*, 819–823. https://doi.org/10.1126/science.1231143.

49. Stewart, S.A., Dykxhoorn, D.M., Palliser, D., Mizuno, H., Yu, E.Y., An, D.S., Sabatini, D.M., Chen, I.S.Y., Hahn, W.C., Sharp, P.A., et al. (2003). Lentivirus-delivered stable gene silencing by RNAi in primary cells. RNA *9*, 493–501. https://doi.org/10.1261/rna.2192803.

50. Li, H., and Durbin, R. (2009). Fast and accurate short read alignment with Burrows-Wheeler transform. Bioinformatics *25*, 1754–1760. https://doi.org/10.1093/bioinformatics/btp324.

51. Li, H., Handsaker, B., Wysoker, A., Fennell, T., Ruan, J., Homer, N., Marth, G., Abecasis, G., and Durbin, R.; 1000 Genome Project Data Processing Subgroup (2009). The Sequence Alignment/Map format and SAMtools. Bioinformatics *25*, 2078–2079. https://doi.org/10.1093/bioinformatics/btp352.

52. Zhang, Y., Liu, T., Meyer, C.A., Eeckhoute, J., Johnson, D.S., Bernstein, B.E., Nusbaum, C., Myers, R.M., Brown, M., Li, W., and Liu, X.S. (2008). Model-based analysis of ChIP-Seq (MACS). Genome Biol. *9*, R137. https://doi.org/10.1186/gb-2008-9-9-r137.

53. Ramírez, F., Ryan, D.P., Gruning, B., Bhardwaj, V., Kilpert, F., Richter, A.S., Heyne, S., Dundar, F., and Manke, T. (2016). deepTools2: a next generation web server for deep-sequencing data analysis. Nucleic Acids Res. *44*, W160–W165. https://doi.org/10.1093/nar/gkw257.

54. Robinson, J.T., Thorvaldsdóttir, H., Winckler, W., Guttman, M., Lander, E.S., Getz, G., and Mesirov, J.P. (2011). Integrative genomics viewer. Nat. Biotechnol. *29*, 24–26. https://doi.org/10.1038/nbt.1754.

55. Heinz, S., Benner, C., Spann, N., Bertolino, E., Lin, Y.C., Laslo, P., Cheng, J.X., Murre, C., Singh, H., and Glass, C.K. (2010). Simple combinations of lineage-determining transcription factors prime cis-regulatory elements required for macrophage and B cell identities. Mol. Cell *38*, 576–589. https://doi.org/10.1016/j.molcel.2010.05.004.

56. Ross-Innes, C.S., Stark, R., Teschendorff, A.E., Holmes, K.A., Ali, H.R., Dunning, M.J., Brown, G.D., Gojis, O., Ellis, I.O., Green, A.R., et al. (2012). Differential oestrogen receptor binding is associated with clinical outcome in breast cancer. Nature *481*, 389–393. https://doi.org/10.1038/nature10730.

57. Mei, S., Qin, Q., Wu, Q., Sun, H., Zheng, R., Zang, C., Zhu, M., Wu, J., Shi, X., Taing, L., et al. (2017). Cistrome Data Browser: a data portal for ChIP-Seq and chromatin accessibility data in human and mouse. Nucleic Acids Res. *45*, D658–D662. https://doi.org/10.1093/nar/gkw983.

58. Cornwell, M., Vangala, M., Taing, L., Herbert, Z., Köster, J., Li, B., Sun, H., Li, T., Zhang, J., Qiu, X., et al. (2018). VIPER: Visualization Pipeline for RNA-seq, a Snakemake workflow for efficient and complete RNA-seq analysis. BMC Bioinf. *19*, 135. https://doi.org/10.1186/s12859-018-2139-9.

59. Dobin, A., Davis, C.A., Schlesinger, F., Drenkow, J., Zaleski, C., Jha, S., Batut, P., Chaisson, M., and Gingeras, T.R. (2013). STAR: ultrafast universal RNA-seq aligner. Bioinformatics *29*, 15–21. https://doi.org/10.1093/bioinformatics/bts635.

60. Trapnell, C., Williams, B.A., Pertea, G., Mortazavi, A., Kwan, G., van Baren, M.J., Salzberg, S.L., Wold, B.J., and Pachter, L. (2010). Transcript assembly and quantification by RNA-Seq reveals unannotated transcripts and isoform switching during cell differentiation. Nat. Biotechnol. *28*, 511–515. https://doi.org/10.1038/nbt.1621.

61. Love, M.I., Huber, W., and Anders, S. (2014). Moderated estimation of fold change and dispersion for RNA-seq data with DESeq2. Genome Biol. *15*, 550. https://doi.org/10.1186/s13059-014-0550-8.

62. Chen, X., Janssen, J.M., Liu, J., Maggio, I., t Jong, A.E.J., Mikkers, H.M.M., and Gonçalves, M.A.F.V. (2017). In trans paired nicking triggers seamless genome editing without double-stranded DNA cutting. Nat. Commun. *8*, 657. https://doi.org/10.1038/s41467-017-00687-1.

63. Layer, R.M., Pedersen, B.S., DiSera, T., Marth, G.T., Gertz, J., and Quinlan, A.R. (2018). GIGGLE: a search engine for large-scale integrated genome analysis. Nat. Methods *15*, 123–126. https://doi.org/10.1038/nmeth.4556.

64. Krijger, P.H.L., Geeven, G., Bianchi, V., Hilvering, C.R.E., and de Laat, W. (2020). 4C-seq from beginning to end: A detailed protocol for sample preparation and data analysis. Methods *170*, 17–32. https://doi.org/10.1016/j.ymeth.2019.07.014.

STAR★METHODS

KEY RESOURCES TABLE

REAGENT or RESOURCE	SOURCE	IDENTIFIER
Antibodies		
Rabbit monoclonal anti-AR	Cell Signaling Technology	Cat#5153S; RRID:AB_10692774
Rabbit monoclonal anti-HOXB13	Cell Signaling Technology	Cat# 90944; RRID:AB_2734734
Rabbit polyclonal anti-GATA2	Abcam	Cat# ab109241; RRID:AB_10865130
Rabbit polyclonal anti-TFAP2C	Proteintech	Cat# 14572-1-AP; RRID:AB_2271424
Rabbit monoclonal anti-β-Actin, HRP conjugate	Cell Signaling Technology	Cat#5125S; RRID:AB_1903890
Rabbit monoclonal anti-β-Tubulin, HRP conjugate	Cell Signaling Technology	Cat#5346S; RRID:AB_1950376
Goat anti-rabbit IgG, HRP conjugate	Cell Signaling Technology	Cat# 7074; RRID:AB_2099233
Rabbit polyclonal anti-H3K27ac	Diagenode	Cat# C15410196; RRID:AB_2637079
Rabbit polyclonal anti-FOXA1	Abcam	Cat#ab23738; RRID:AB_2104842
Biological samples		
Patient Derived Xenografts (PDX)	University of Washington	LuCap
Chemicals, peptides, and recombinant proteins		
Enzalutamide	Selleck	Cat#1250
Critical commercial assays		
NEBNext UltraII DNA Library Prep Kit	NEB	Cat#E7645S
Diagenode ATAC-seq kit	Diagenode	Cat#C01080002
Deposited data		
ChIP-seq raw and processed data	This paper	GEO: accession GSE276052
ATAC-seq raw and processed data	This paper	GEO: accession GSE276052
4C-seq raw and processed data	This paper	GEO: accession GSE276052
RNA-seq raw and processed data	This paper	GEO: accession GSE276052
Experimental models: Cell lines		
LNCaP	ATCC	Cat#CRL-1740
LNCaP-AR-GFP	This paper	N/A
MDA-PCa-2b	ATCC	Cat# CRL-2422, RRID:CVCL_4748
VCaP16	Poluben et al.[29]	N/A
293T	ATCC	Cat#CRL-3216
Experimental models: Organisms/strains		
NSG Mice	Charles River	Strain Code 614
Oligonucleotides		
ON-TARGET SMARTpool siRNA nontargeting control	Horizon	Cat# D-001810-10-05
ON-TARGET SMARTpool AR siRNA	Horizon	Cat#L-003400-00-0005
ON-TARGET SMARTpool HOXB13 siRNA	Horizon	Cat#L-012226-00-0005
ON-TARGET SMARTpool GATA2 siRNA	Horizon	Cat#L-009024-02-0005
ON-TARGET SMARTpool TFAP2C siRNA	Horizon	Cat#L-005238-00-0005
ON-TARGET SMARTpool DOT1L siRNA	Horizon	Cat#L-014900-01-0005
ON-TARGET SMARTpool CTCF siRNA	Horizon	Cat#L-020165-00-0005
ON-TARGET SMARTpool NCOA1 siRNA	Horizon	Cat#L-005196-00-0005
ON-TARGET SMARTpool PA2G4 siRNA	Horizon	Cat#L-008860-00-0005
ON-TARGET SMARTpool U2AF1 siRNA	Horizon	Cat#L-012325-01-0005
ON-TARGET SMARTpool FOXA1 siRNA	Horizon	Cat#L-010319-00-0005

(*Continued on next page*)

Continued

REAGENT or RESOURCE	SOURCE	IDENTIFIER
See Table S1 for CRISPR screening library	This paper	N/A
See Table S3 for primers for qPCR, CRISPRi gRNAs, shRNAs, 4C-seq primers	This paper	N/A
Recombinant DNA		
pX335-U6	Cong et al.[48]	Addgene Plasmid #42335
pDONOR-221	Thermofisher	Cat#12536017
pCMV-VSV-G packaging plasmid	Stewart et al.[49]	Addgene Plasmid #8454
psPAX2 packaging plasmid	Didier Trono	Addgene Plasmid #12260
pLEX_304-HOXB13	This paper	N/A
pLEX_304-GATA2	This paper	N/A
pLEX_304-TFAP2C	This paper	N/A
Software and algorithms		
BWA	Li et al.[50]	https://bio-bwa.sourceforge.net/
Samtools	Li et al.[51]	http://www.htslib.org/
Picard	Broad Institute	https://broadinstitute.github.io/picard/
MACS2	Zhang et al.[52]	http://liulab.dfci.harvard.edu/MACS/
Deeptools	Ramirez et al.[53]	http://deeptools.readthedocs.io/en/latest/
IGV	Robinson et al.[54]	http://software.broadinstitute.org/software/igv/
Homer	Heinz et al.[55]	http://homer.ucsd.edu/homer
Diffbind	Ross-Innes et al.[56]	http://bioconductor.org/packages/release/bioc/vignettes/DiffBind/inst/doc/DiffBind.pdf
pheatmap	Raivo Kolde	https://cran.r-project.org/web/packages/pheatmap/pheatmap.pdf
Cistrome DB	Mei et al.[57]	http://dbtoolkit.cistrome.org
VIPER RNA-seq pipeline	Cornwell et al.[58]	https://bitbucket.org/cfce/viper
STAR	Dobin et al.[59]	https://github.com/alexdobin/STAR
Cufflinks	Trapnell et al.[60]	http://cole-trapnell-lab.github.io/cufflinks/tools/
DESEQ2	Love et al.[61]	https://bioconductor.org/packages/release/bioc/vignettes/DESeq2/inst/doc/DESeq2.html
PoolQ	The Broad Institute	https://portals.broadinstitute.org/gpp/public/software/poolq
STARS software	The Broad Institute	https://portals.broadinstitute.org/gpp/public/software/stars
fsgsea	Korotkevich et al.	https://bioconductor.org/packages/release/bioc/manuals/fgsea/man/fgsea.pdf
Custom code to map peaks to genes	This paper	Zenodo: https://doi.org/10.5281/zenodo.14721032.

EXPERIMENTAL MODEL AND STUDY PARTICIPANT DETAILS

Cell lines

LNCaP, MDA-PCa-2b, and 293T cell lines were purchased from ATCC and grown in media specified by ATCC: RPMI with 10% fetal calf serum (Gibco) for LNCaP, DMEM with 10% fetal calf serum (Gibco) for 293T, F-12K Medium with 20% fetal calf serum (Gibco), 25 ng/mL cholera toxin (Sigma), 10 ng/mL mouse EGF (Corning), 0.005 mM phosphoethanolamine (Sigma), 100 pg/mL hydrocortisone (Sigma), 45 nM sodium selenite (Sigma), and 0.005 mg/mL human recombinant insulin (Thermofisher) for MDA-PCA-2b. VCaP16 cells were a kind gift from Steve Balk[29] and grown in DMEM with 10% fetal calf serum (Gibco) supplemented with 16 μM

enzalutamide (Selleck). VCaP16 cell line was made resistant to enzalutamide by repeated passaging in increasing drug concentrations. All cell lines were authenticated by short tandem repeat profiling (Laragen) and tested negative for mycoplasma (ATCC).

PDX samples

The LuCaP PDXs were propagated in male NOD SCID gamma (NSG) mice obtained from the NCI Division of Cancer Treatment and Diagnosis (DCTD) Frederick, MD. The LuCaP PDX series was derived from human donors who had signed written informed consent under the aegis of the Prostate Cancer Donor Program at the University of Washington and has been previously characterized.[25] Experiments were conducted under the NCI Animal Care and Use Committee-approved protocol (Animal Study Number LGCP-003) in accordance with ACUC recommendations. Six-week-old male NSG mice were subcutaneously injected with 2 million processed PDX tumor cells and tumor measurements taken weekly using digital calipers and harvested when the tumor reached 2000 cubic millimeters. Tumor identities were confirmed by short tandem repeat profiling (Laragen) and tested negative for mycoplasma (ATCC).

METHOD DETAILS

Creation of reporter cell line LNCaP-AR-GFP

The AR reporter cell line was generated by homology directed repair (HDR) using the CRISPR in trans paired nicking strategy.[62] A gRNA targeting near the stop codon of the endogenous AR (sequence: TAGGGTTTCCAATGCTTCAC hg19 chrX: 66943669–66943688) was cloned into the pX335-U6 plasmid (Addgene 42335) that also expresses SpCas9 nickase. The HDR repair plasmid was designed to replace the stop codon with an IRES followed by GFP, 2A peptide cleavage sequence, and hygromycin selection marker. The PEST protein degradation sequence was included to reduce the half-life of GFP protein. The homology arms corresponded to the genomic sequences approximately 1 kb surrounding the stop codon of AR (hg 19 chrX: 66942770–66943680 and chrX: 66943684–66944748, respectively).

Assembly of the HDR plasmid was done by sequential ligations of synthesized gblocks and PCR products. A gblock (IDT) corresponding to 66943463–66943680 of the left homology arm (contains an endogenous NheI site at the 5′ end) followed by IRES-GFP was first cloned into the NheI-BamHI sites of pDONR-221 (Thermofisher). A second gblock with a BamHI site followed by hygromycin resistance gene and genomic sequence 66943684–66943834 (contains endogenous EcoRI site at 3′ end) was then cloned into the BamHI-EcoRI site. PCR was used to amplify the remaining homology arm genomic sequences from LNCaP genomic DNA using primers appended with appropriate restriction enzyme sites and gRNA targeting sequence. The right arm was cloned using EcoRI-SalI sites and the left arm using the NheI site.

Nucleofection of LNCaP cells was performed using the Nucleofector instrument according to manufacturer's instructions (Lonzo). Approximately 1 week after nucleofection, positive clones were selected by hygromycin (50 ng/mL) and single cell clones isolated by limiting dilution. AR dependent GFP expression was confirmed by immunoblotting and FACS.

Design and creation of transcription factor gRNA library

The initial list of human transcription factors was downloaded from humantfs.ccbr.utronot.ca. This curated list includes 1,639 transcription factors compiled from literature and computational inference.[16] For each factor, we designed 4 gRNAs using the Broad Institute's CRISPick design tool (portals.broadinstitute.org/gppx/crispick/public). There were 5 genes for which there was no solution (AC008770.3, AC023509.3, AC092835.1, AC138696.1, DUX3) and were excluded. The library included 500 nontargeting gRNA as negative controls, and 10 gRNAs targeting AR as positive controls. To account for effects related to cell death, we included 40 gRNAs targeting the common essential genes RPL23, SF3B3, and EIF4A3. Taken together the library consisted of 7,076 gRNAs and the list of genes and gRNA sequences are listed in Table S1 (Note, there are 7,075 unique gRNAs as NANOG and NANOGP8 had overlapping gRNA sequences). The gRNAs were synthesized as an oligonucleotide pool from Genscript appended with sequences for PCR amplification and Golden Gate cloning into pXPR_BRD003 using Esp3I (New England Biolabs). The plasmid pool was transformed into Stbl4 electrocompetent cells (Thermofisher) and DNA purified using Qiagen Maxiprep kit.

Pooled lentivirus CRISPR screen for *trans*-acting factors

Lentivirus was generated by transfecting 293T cells with the library pool with the packaging plasmids pCMV-VSV-G (Addgene 8454) and psPAX2 (Addgene 1226) using the TransIT-LT1 transfection reagent (Mirius). Supernatant was collected after 48 h, filtered through 0.45 μm filter (Millipore), and stored at −80°C. LNCaP-AR-GFP cells stably expressing Cas9 were transduced in the presence of 4 μg/mL polybrene followed by selection with 2 μg/mL puromycin for 3 days. The optimal virus concentration was determined by titrating the volume of virus to obtain an infection efficiency of approximately 30% by measuring viability in the absence and presence of puromycin. This corresponds to a multiplicity of infection <1 to ensure each cell receives no more than one gRNA. For each replicate, 27 million cells were transduced which corresponds to a representation of approximately 3,000 cells per gRNA. We performed two biological replicates of each screen.

Cells were harvested 7 days after infection for sorting on a Sony MA900 Cell Sorter. We used LNCaP cells with no GFP expression as a reference to gate GFP positive cells. We binned cells based on GFP signal and collected 1 million cells for each bin corresponding to 0–10%, 10–20%, 80–90%, and 90–100%. Unsorted cells were used as a total library pool control. Genomic DNA was purified

using Monarch Genomic DNA Purification Kit (New England Biolabs). Sequencing libraries were generated by PCR amplification of genomic DNA using construct specific primers containing Illumina adaptor sequences and barcodes for multiplexing. PCR product was confirmed by agarose gel electrophoresis. The libraries were pooled, purified using Ampure XP beads (Beckman), and submitted for sequencing on Illumina MiniSeq with 35 million 75 bp single end reads.

Analysis of Pooled Screen Data

Alignment of the FASTQ files to the library was performed using the Poolq tool (Broad Institute, version 2.2.0). The absolute reads for the 0%–10% and 10%–20% bins were pooled to generate the 0%–20% fraction and likewise for the 80%–90% and 90%–100% bins to create the 80%–100% fraction. The reads were normalized using the total number of reads per sample and averaged between replicates. Normalized reads were converted to log2 CPM values by multiplying reads by 1 million, adding 1, and taking the log2. The differential log2 score represents the log2 for 0%–20% subtracted from 80% to 100%. We determined significant hits for further study using the STARS algorithm (Broad Institute, version 1.3) with a null distribution set to 1000 iterations.

siRNA experiments

Cells were plated one day prior to transfection with ON-TARGETplus siRNA (Dharamcon) consisting of a pool of 4 individual siRNAs targeting each gene or nontargeing control at a dose of 25 pmol per well of a 6-well plate using RNAiMax (ThermoFisher). Cells were harvested 48 h after transfection.

CRISRPi rescue experiments

Cells were plated one day prior to transduction with lentiviruses expressing dCas9-KRAB and gRNA targeting the transcription start site (Table S3) and open reading frame of indicated gene in the presence of 4 μg/mL polybrene (Sigma). A nontargeting gRNA and LacZ open reading frame were used as negative controls. Since the rescue construct is driven by an exogenous promoter there was no overlap with the gRNA targeting the endogenous gene. Media was replaced after 24 h and cells harvested 72 h after transduction for immunoblotting and quantitative RT-PCR.

shRNA experiments

Cells were plated one day prior to transduction with lentivirus expressing shRNAs targeting GATA2 or a nontargeting control in the presence of 4 μg/mL polybrene (Sigma) (Table S3). Media was replaced after 24 h and cells harvested 72 h after transduction for immunoblotting and quantitative RT-PCR.

Quantitative RT-PCR

RNA was isolated using RNeasy Plus Kit (Qiagen) and cDNA synthesized using Protoscript First Strand cDNA Synthesis Kit (New England Biolabs). Quantitative PCR was performed on a Quantstudio 5 using SYBR green (ThermoFisher). Primers used for quantitative RT-PCR are listed in Table S3. AR was used as a positive control, U2AF1 was used a control for an essential gene to rule out effects due to nonspecific cell death, and FOXA1 was used as a control for a transcription factor that binds the AR enhancer but did not score in the screen.

Immunoblotting

Cells were lysed with RIPA buffer (Sigma) and quantified by BCA assay (ThermoFisher). Equal amounts of protein were loaded onto 4%–12% Bis-Tris NuPage gel (ThermoFisher) and immunoblotting performed per standard protocol. Antibodies used: Androgen Receptor (Cell Signaling Technology, cat#5153), HOXB13 (Cell Signaling Technology, cat#90944), GATA2 (Abcam, cat#ab109241), TFAP2C (Proteintech cat#14572-1-AP), Beta-Actin-HRP (Cell Signaling Technology, cat#5125), Beta-Tubulin-HRP (Cell Signaling Technology, cat#5346), Goat anti-Rabbit HRP (Cell Signaling Technology, cat#7074).

Cell line and tissue ChIP

For cell lines, approximately 10 million cells were fixed using 2 mM DSG (CovaChem) for 10 min followed by 1% formaldehyde for 10 min at 37°C and quenched with 2 M glycine for 5 min at room temperature. For tissue samples, approximately 20 mg of frozen tissue was pulverized with Covaris Cryoprep (level 4 × 2 times), resuspended in 5 mL PBS, and fixed with 2 mM DSG (CovaChem) for 10 min at 37°C followed by 1% formaldehyde for 10 min at 37°C and quenched with 2 M glycine for 5 min at room temperature. Cross-linked cells were resuspended in cold lysis buffer (50 mM Tris pH 8.0, 10 mM EDTA pH 8.0, 0.5% SDS, 1X protease inhibitor cocktail) and sheared using a Bioruptor Pico (Diagenode) device. Fragmented chromatin was incubated with 3 μg of H3K27ac (Diagenode, cat#C15410196), GATA2 (Abcam, cat#ab109241), HOXB13 (Cell Signaling Technology, cat#90944), TFAP2C (Proteintech, catalog#14572-1-AP), or FOXA1 (Abcam, cat#ab23738) antibody overnight at 4°C. 5% of each sample prior to addition of antibody was used as an input control. Protein A/G beads (ThermoFisher) were added and incubated for 1 h at 4°C, washed six times with RIPA buffer (50 mM HEPES pH 7.5, 1 mM EDTA pH 8.0, 500 mM LiCl, 0.7% sodium deoxycholate, 1% NP40), and eluted in elution buffer (100 mM $NaHCO_3$, 1% SDS). Samples, including input DNA, were treated with RNase A (ThermoFisher) for 30 min at 37°C followed by proteinase K (New England Biolabs) overnight at 65°C to reverse crosslinking. ChIP DNA was purified with Monarch Genomic DNA Purification Kit (New England Biolabs) and concentrations were quantified by

Qubit fluorometer (ThermoFisher) and TapeStation (Agilent). For ChIP-seq, sequencing libraries were prepared by NEBNext UltraII DNA Library Prep Kit (New England Biolabs) per manufacturer's instructions and sequenced on the Illumina NextSeq2000 platform. For ChIP-qPCR, DNA was quantified using SYBR green (ThermoFisher) on a Quantstudio 5 instrument. Primers used are listed in Table S3.

ATAC-seq

ATAC-seq was performed using the Diagenode ATAC-seq kit according to manufacturer's manual. Nuclei were isolated from 50,000 cells by incubating with digitonin containing lysis buffer for 3 min on ice followed by tagmentation at 37°C for 30 min. Following DNA purification, indexes were added by PCR after determining optimal number of cycles by qPCR. Library quality was assessed by TapeStation (Agilent) and sequenced on the Illumina NextSeq2000 platform.

RNA-seq

RNA was extracted from cells using RNeasy Plus RNA kit (Qiagen) from 4 biological replicates. RNA concentration and integrity were assessed by TapeStation (Agilent). Samples were submitted to Novogene for mRNA library construction and sequencing on Illumina Novaseq X Plus. Demultiplexed FASTQ files were analyzed using the VIPER pipeline workflow.[58] Reads were aligned to build hg19 using STAR and cufflinks used to generate normalized read counts in FPKM. Differential expression was determined using DESeq2 as part of the VIPER pipeline. Unsupervised clustering of RNA-seq data was done by Pearson correlation using the pheatmap R package with the top 1000 variably expressed genes as defined by median absolute deviation. GSEA was performed using the fsgsea R package using the Broad Institute "H: hallmark gene set."

ChIP-seq and ATAC-seq data analysis

Reads were aligned to build hg19 after filtering for ENCODE blacklist regions using bwa (0.7.17) and converted to BAM format using Samtools (1.17). Duplicate reads were removed using Picard (2.27.3) and peaks identified with MACS2 (2.2.7.1) using input controls with a q-value cutoff of 0.01. Input subtracted bigWig files were generated using Deeptools (3.5.1) for visualization in IGV. Quality assessment included sequence quality scores, non-redundant fraction, fraction of reads falling within peak regions, overlap with known DNase I hypersensitivity sites derived from ENCODE, and motif enrichment by Homer. The Bioconductor package DiffBind (3.10.1) was used to identify condition-specific peaks with an FDR <0.05 using at least two biological replicates. Unsupervised clustering of ChIP-seq data was done by Pearson correlation using the pheatmap R package with the top 2000 variable peaks as defined by median absolute deviation. Cistome DB toolkit (http://dbtoolkit.cistrome.org) was used to quantify (GIGGLE score) the overlap of ChIP-seq data with published datasets that were run through a standardized pipeline.[63]

Scanning motif analysis

The web version of Find Individual Motif Occurrences (FIMO) https://meme-suite.org/meme/doc/fimo.html was used to scan for motifs using the Jaspar database of motifs with a *p*-value cutoff of 0.001.

4C-seq

4C libraries were prepared as previously described.[64] Briefly, 10 million cells were cross-linked with 2% formaldehyde for 10 min at room temperature and quenched with 2 M glycine. Samples were resuspended in lysis buffer (50 mM Tris pH 7.5, 5 mM EDTA pH 8, 150 mM NaCl, 0.5% NP-40, 1% Triton X-100) and incubated on ice for 20 min followed by addition of SDS (0.3% final) and incubation at 37°C for 1 h. Triton X-100 was added (2.5% final) and incubated for 37°C for 1 h. Samples were then digested with DpnII (New England Biolabs) overnight, followed by ligation overnight and reverse crosslinking and DNA purification. Second digestion and ligation were done similarly with NlaIII (New England Biolabs). Libraries were generated using two-step PCR strategy. The first PCR is an inverse PCR using enhancer or promoter viewpoint specific primers (Table S3). The second PCR incorporates the indexed Illumina sequencing adaptors. Library quality was assessed by TapeStation (Agilent) and sequenced on the Illumina NextSeq2000 platform. 4C-seq was analyzed using a previously published workflow[64] that intersects mapped reads with an in silico generated fragmented genome. Read counts are normalized and smoothed using a running mean to generate bigwig files for visualization in IGV.

Linking HiChIP data to genes

ChIP-seq peaks called by MACS2 were extended upstream and downstream by 5 kb and intersected with HiChIP data from LNCaP cells[35] to identify interacting regions. A gene was considered to interact with the peak if the interacting region was within 5 kb of the gene's transcriptional start site. Gene annotations RefSeqAll (ncbiRefSeq) hg19 were used for genome annotations.

QUANTIFICATION AND STATISTICAL ANALYSES

CRISPR-Cas9 screen

Statistical analyses were performed using the STARS algorithm (Broad Institute, version 1.3). The statistical details including sample size and statistical tests are described in Methods Details. Significance is defined as an adjusted FDR <0.01.

Quantitative RT-PCR experiments

Statistical analyses were determined using R (version 4.4.1). Sample size, statistical tests, and precision measures are indicated in figure legends. Significance was defined as a p-value <0.05.

ChIP-seq and ATAC-seq experiments

Peak calling was performed using MACS2 (version 2.2.7.1) using input controls with a q-value cutoff of 0.01 to define a significant peak. Statistical details including sample size and statistical tests are described in Method Details. Differential peaks were determined using the Diffbind R package (version 3.10.1). Statistical details are described in Method Details. Significance was defined based on an FDR <0.05.

RNA-seq experiments

Statistical analyses were performed using the VIPER pipeline[58] which uses DESEQ2 to call differentially expressed genes. Statistical details include sample size and statistical tests are described in Method Details. Significant genes were defined based on an FDR <0.05 and fold change >2.